*American Mineralogist, Volume 85, pages 514–523, 2000*

# Equation of state of magnetite and its high-pressure modification: Thermodynamics of the Fe-O system at high pressure

CAMILLA HAAVIK,[1] SVEIN STØLEN,[1,]* HELMER FJELLVÅG,[1] MICHAEL HANFLAND,[2] AND DANIEL HÄUSERMANN[2]

[1]Department of Chemistry, University of Oslo, Postbox 1033, N-0315 Oslo, Norway
[2]European Synchrotron Radiation Facility, B.P. 220, F-38043 Grenoble, France

## ABSTRACT

$Fe_3O_4$ has been studied by high-pressure diffraction to 43 GPa. No major changes in the spinel-type structure of magnetite is observed below 21.8 GPa. At higher pressure a sluggish transition to a high-pressure modification, h-$Fe_3O_4$, is observed. The X-ray diffraction pattern of the high-pressure modification is consistent with the orthorhombic unit cell ($CaMn_2O_4$-type structure, space group *Pbcm*) recently proposed for h-$Fe_3O_4$ by Fei et al. (1999), however, it is also consistent with a more symmetric $CaTi_2O_4$-type structure (space group *Bbmm*). Bulk modulus values for magnetite, $K_{T0}$ = 217 (2) GPa, and h-$Fe_3O_4$, $K_{T0}$ = 202 (7) GPa, are calculated from the pressure-volume data using a third-order Birch-Murnaghan equation of state. A thermodynamic analysis of the Fe-O system at high pressure is presented. The proposed equation of state of h-$Fe_3O_4$ gives an increased stability of wüstite relatively to a two-phase mixture of iron and h-$Fe_3O_4$ compared to earlier equations of state and removes an inconsistency in the thermodynamic description of the Fe-O system at high pressure.

## INTRODUCTION

Magnetite is, at ambient pressure and low temperature, a ferrimagnetic inverse spinel where the tetrahedral positions are occupied by $Fe^{3+}$ and the octahedral sites contain equal amounts of $Fe^{3+}$ and $Fe^{2+}$ (Fleet 1981). Three transformations are observed with increasing temperature. The Verwey transition at 119 K is related to a change in the degree of electron localization of the iron atoms (Verwey 1939) and fast electron exchange between the octahedral $Fe^{2+}$ and $Fe^{3+}$ is observed above the transition temperature. Transport-property measurements indicate that the charge distribution depends on temperature and a gradual disordering of the inverse spinel toward a random one is observed with increasing temperature (Wu and Mason 1981). Magnetite becomes paramagnetic at $T_C$ = 848.5 K (Grønvold and Sveen 1974).

The high-pressure modification of magnetite, h-$Fe_3O_4$, which slowly appears at pressures above ≈25 GPa (Mao et al. 1974), is paramagnetic at ambient temperature (Pasternak et al. 1994). The density of h-$Fe_3O_4$ was first estimated from the tentative unit-cell assignment by Mao et al. (1974), based on an insufficient number of diffraction lines for monoclinic symmetry. It was argued that the calculated density indicates that all iron atoms are in sixfold coordination (Mao et al. 1974). This would require a massive reconstructive transition from the low-pressure spinel-type structure where iron is partly fourfold and partly sixfold coordinated. A recent Mössbauer spectroscopy study (Pasternak et al. 1994) on the other hand indicates that the Fe atoms remain in their original coordination environments in the high-pressure modification, and suggests that the transition involves a distortion of the tetrahedra and octahedra of the low pressure structure only. A smaller volume decrement connected with the magnetite to h-$Fe_3O_4$ transition than suggested by Mao et al. (1974) is, hence, indicated. Recently Fei et al. (1999) proposed that h-$Fe_3O_4$ takes the $CaMn_2O_4$-type structure (*Pbcm*) where $Fe^{3+}$ is octahedrally coordinated and $Fe^{2+}$ is eightfold coordinated (bicapped trigonal prismatic). With this structure assignment h-$Fe_3O_4$ is about 6.5% more dense than magnetite at 24 GPa. In earlier thermodynamic evaluations of the Fe-O system (Saxena et al. 1993; Fabrichnaya and Sundman 1997) a large volume decrement for the transformation from magnetite to h-$Fe_3O_4$ is used which implies a considerable increase in the stability of magnetite at high pressure compared to that obtained by extrapolation using the volume of the low-pressure structure. A large volume decrement for the transformation results in a disproportion of wüstite, $Fe_{1-y}O$, to iron and magnetite at high pressure (Huang and Bassett 1986; Stølen and Grønvold 1996). This conclusion contradicts phase diagram studies which show that NaCl-type wüstite is stable to pressures near 70 GPa at 1000 K where after the NaCl-type structure transforms to a NiAs-type structure (Fei and Mao 1994).

The mechanism of the transformation is not clear. Magnetite and h-$Fe_3O_4$ are reported to coexist as a two-phase mixture over several GPa (Mao et al. 1974; Huang and Bassett 1986; Pasternak et al. 1994) and the transition, hence, appears to be of first order. The transition is not related to the Verwey transition because $T_V$ decreases with *P* (Ramasesha et al. 1994). For pressures up to 66 GPa, Mössbauer spectra characteristic of divalent iron were not detected (Pasternak et al. 1994). Hence,

*E-mail: svein.stolen@kjemi.uio.no

0003-004X/00/0304–514$05.00 

the fast electron exchange between $Fe^{2+}$ and $Fe^{3+}$, characteristic of magnetite above the Verwey transition, is still present. The small change in magnitude of the resistivity connected with the pressure induced transition supports this conclusion (Morris and Williams 1997). High pressure single-crystal diffraction data up to 4.5 GPa at ambient temperature (Finger et al. 1986) show no evidence of any valence disordering between tetrahedral and octahedral sites. Furthermore, in that pressure range both the tetrahedra and the octahedra display the bulk modulus characteristic for the unit-cell volume. The oxygen *x*-coordinate, the only variable atomic position coordinate for the spinel structure, does not vary with pressure for $P < 4.5$ GPa (Finger et al. 1986; Nakagiri et al. 1986).

The present investigation reports an improved equation of state for magnetite and proposes an equation of state for h-$Fe_3O_4$ based on the $CaMn_2O_4$-type structure (Fei et al. 1999). Alternative descriptions of the crystal structure of h-$Fe_3O_4$ are discussed. The calculated phase relations in the Fe-O system at high pressure are in better agreement with experiments than earlier evaluations (Huang and Bassett 1986; Saxena et al. 1993; Fabrichnaya and Sundman 1997).

## EXPERIMENTAL METHODS

### Sample preparation and characterization

The sample was prepared from $Fe^{3+}$ oxide (pro analysi, E. Merck No. 3924) and iron. Prior to use $Fe_2O_3$ was heated in a furnace at 1273 K until a constant mass was attained. A small part of the sample was reduced to Fe in dry hydrogen gas at 1073 K for 6 h and afterward crushed to a fine powder. Stoichiometric amounts of the resulting iron and $Fe_2O_3$ were heated in evacuated and sealed vitreous silica tubes at 1273 K for 2 days and cooled with the furnace. X-ray powder diffraction showed only reflections from $Fe_3O_4$. The resulting unit-cell constant, $a$ = 839.65 (7) pm, is in good agreement with Fleet (1981).

### High-pressure technique

The high-pressure measurements were performed at room temperature in a membrane-type diamond anvil cell with the sample loaded in a hole in a stainless steel gasket with a diameter of 125 μm and an initial thickness of 40 μm. $N_2$ was used as pressure transmitting medium. It solidifies at 2.3 GPa at ambient temperature. Weak reflections from solid $N_2$ were thus observed in several sets of data. Three crystalline modifications of $N_2$ are reported at high pressure. The disordered hexagonal low-pressure structure (Streib et al. 1962) transforms to a disordered cubic structure between 4 and 5 GPa (Cromer et al. 1981) which again transforms to an ordered rhombohedral modification near 16 GPa (Mills et al. 1986). The rhombohedral modification is stable at least to 44 GPa (Olijnyk 1990). Pressure was measured by the ruby fluorescence technique using the non-linear hydrostatic pressure scale (Mao et al. 1986).

The powder X-ray diffraction data were collected on beamline ID9 at the European Synchrotron Radiation Facility (ESRF). The diffractograms were collected on an image plate, scanned and thereafter integrated with the computer program FIT2D (Hammersley et al. 1996) and thereby transformed to a one-dimensional data set. The monochromator was a single reflection Si (111) monochromator with wavelength $\lambda$ = 47.60 (4) pm. The 2D-image plate distance and the wavelength were calibrated using Si (Deslattes and Henins 1973) as an external calibration source. The conical opening of the pressure cell allowed the observation of the full diffraction rings for $d > 95$ pm.

Rietveld refinement of the crystal structure of magnetite at the different pressures was done by means of the GSAS (Larson and von Dreele 1986) package. The background was described by means of 9-term cosine Fourier series polynomials and the peak shape by a Gaussian-Lorentzian function (5 parameters). In addition the zero point, one unit-cell dimension, one atomic coordinate parameter and isotropic displacement factors were refined, altogether 17 to 19 variables. The $2\theta$ range ≈5–25° was used, containing ≈1100 data points and 14 contributing Bragg reflections. The diffraction data for h-$Fe_3O_4$ were analyzed assuming a two-phase mixture with magnetite. Different structural models were considered. Soft distance restraints were introduced for the Fe-O separations in the $CaTi_2O_4$-type structure model, see below.

## RESULTS AND DISCUSSION

A three-dimensional representation of the X-ray diffractograms recorded on increasing pressure ($P_{max}$ = 40 GPa) is given in Figure 1. Weak reflections from solid $N_2$ (cubic) are present in the diagrams at pressure above 3.4 GPa, see e.g., the small peak at around $2\theta$ = 10° for $P$ = 3.4 to 13.5 GPa. At higher pressure this peak overlaps with the magnetite 311 line. No major changes in the spinel-type structure are observed below 21.8 GPa. At higher pressure the intensities of the char-

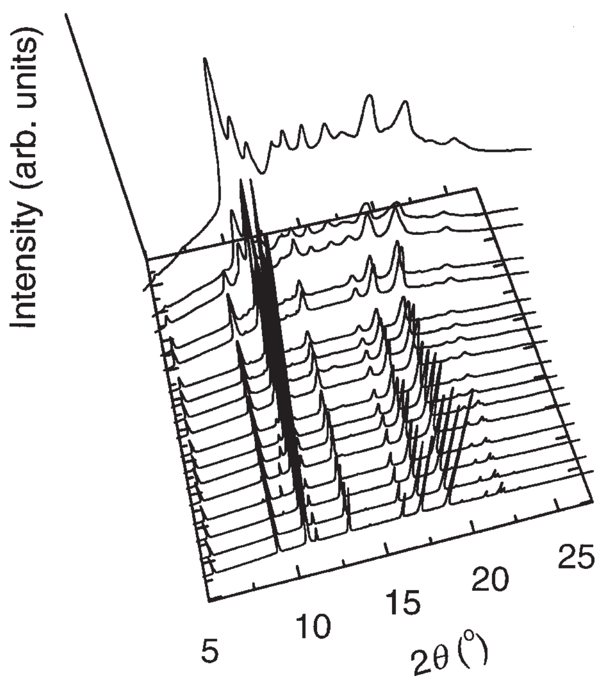


**FIGURE 1.** Observed XRD patterns of $Fe_3O_4$ taken at 1.4, 2.3, 3.4, 6.6, 8.3, 11.3, 12.5, 13.5, 15.7, 17.5, 19.4, 21.8, 24.2, 26.9, 30.3, 35.2, and 40.0 GPa. The lowest pressure diagram is in front. $\lambda$ = 47.60 pm.

acteristic magnetite reflections are reduced and those of the high-pressure modification evolve gradually. Reflections that can be ascribed to magnetite appear to be present at least up to 30.3 GPa and the slow kinetics of the transformation (e.g., Mao et al. 1974) is confirmed. The slow kinetics is also seen during decompression for diffractograms recorded at 30, 24, 19, 12, and 6 GPa. Hysteresis is observed and h-$Fe_3O_4$ does not revert completely to magnetite even at 6 GPa.

The structural transformation is apparently accompanied by a gradual increase in non-coherent scattering and the quality of the diffractograms deteriorates. The change in the diffractograms may in part relate to the fact that the transformation involves atomic motion and/or large strain which reduces the long-range order. Alternatively, this effect may be related to a deformation of the gasket. Even though the non-coherent scattering increases with increasing pressure, the peak shape seems to develop reasonably. The full peak width at half maximum (FWHM) intensity for the magnetite 111 line increases with a constant slope with increasing pressure (Fig. 2a). A similar observation is made

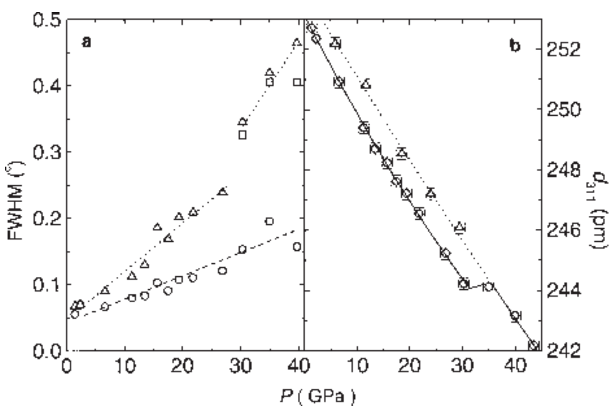


**FIGURE 2.** (**a**) Full peak width at half maximum intensity (FWHM) as a function of pressure. Circles = magnetite 111; triangles = magnetite 311; squares = the d ≈ 258 pm reflection for h-$Fe_3O_4$. (**b**) The *d*-value of magnetite 311. Circles = magnetite 311 on compression; triangles = magnetite 311 on decompression.

for the magnetite 311 line (Fig. 2a) for $P < 25$ GPa. At higher pressure a change in slope of the FWHM for what appears to be magnetite 311 is observed. In this pressure range, the FWHM shows a pressure dependence similar to that for the $d \approx 257$ pm reflection (open squares) which for certain can be assigned to h-$Fe_3O_4$. Above 25 GPa the apparent magnetite 311 seems therefore to contain a major component from the high-pressure modification. An apparent jump in the *d*-value of magnetite 311 at around 30 GPa substantiates this argument, see Figure 2b. The *d*-value for the apparent magnetite 311 on decompression suggests that this reflection contains major components from the high-pressure modification.

### Crystal structure and equation of state of magnetite

Magnetite is an inverse spinel at ambient pressure and low temperature (Fleet 1981). The ideal spinel structure is cubic with space group $Fd\bar{3}m$ and $Z = 8$. Using the centrosymmetric description of the space group the tetrahedral cations are located at (1/8,1/8,1/8), the octahedral cations at (1/2,1/2,1/2), and the oxygen atoms at (*x, x, x*), where $x \approx 0.25$. According to Fleet (1981) $x = 0.2549$ (1) at room temperature. Refined structural parameters are in Table 1. A representative diffractogram is in Figure 3.

The oxygen position parameter (*x*) does not vary with pressure within two standard deviations. No change in the cation distribution is indicated, and the inverse spinel modification seems to be stable in the pressure range covered. The reduced volumes presently obtained for magnetite are compared with earlier reported values in Figures 4 and 5.

The different determinations are in reasonable agreement at pressures below ≈25 GPa, although the values by Mao et al. (1974) show a larger spread than the others. The reduced molar volumes reported at high pressure by Mao et al. (1974), and also the value presently deduced from the 30.3 GPa diagram are low compared with the extrapolated curve from the lower pressure determinations. This discrepancy is probably related to wrong peak assignment in the indexing of the two-phase mixture diagrams, and these determinations are, therefore, not included in the equation of state analysis which follows.

The bulk modulus of magnetite was calculated by least-

TABLE 1. Refined structural parameters, selected bond-distances and cation polyhedra volumes

| $P$* GPa | $a$ pm | $x$ | A-O pm | $V_{AO_4} \times 10^{-6}$ pm³ | B-O pm | $V_{BO_6} \times 10^{-6}$ pm³ |
|---|---|---|---|---|---|---|
| 0 | 839.65 (7) | 0.2549 (3)† | 188.9 (1)‡ | 3.460 (8)‡ | 205.9 (1)‡ | 11.61 (2)‡ |
| 1.4 | 838.37 (5) | 0.2554 (4) | 189.4 (6) | 3.48 (3) | 205.1 (3) | 11.48 (6) |
| 2.3 | 836.85 (5) | 0.2550 (4) | 188.4 (6) | 3.43 (3) | 205.2 (3) | 11.48 (6) |
| 3.4 | 835.17 (6) | 0.2548 (3) | 188.7 (5) | 3.39 (3) | 204.9 (3) | 11.44 (5) |
| 6.6 | 831.22 (8) | 0.2549 (3) | 187.1 (5) | 3.36 (2) | 203.8 (3) | 11.25 (5) |
| 8.3 | 829.66 (8) | 0.2549 (3) | 186.7 (5) | 3.34 (2) | 203.4 (3) | 11.19 (5) |
| 11.3 | 826.26 (9) | 0.2549 (3) | 185.9 (4) | 3.30 (2) | 202.6 (3) | 11.06 (5) |
| 12.5 | 825.47 (11) | 0.2547 (4) | 185.4 (6) | 3.27 (3) | 202.6 (3) | 11.06 (6) |
| 13.5 | 823.96 (12) | 0.2543 (4) | 184.5 (6) | 3.22 (3) | 202.5 (3) | 11.05 (6) |
| 15.7 | 823.21 (19) | 0.2548 (4) | 185.1 (6) | 3.25 (3) | 201.9 (3) | 10.95 (6) |
| 17.5 | 821.40 (16) | 0.2552 (4) | 185.3 (6) | 3.26 (3) | 201.2 (3) | 10.82 (6) |
| 19.4 | 818.91 (18) | 0.2555 (4) | 185.1 (6) | 3.25 (3) | 200.3 (3) | 10.68 (6) |
| 21.8 | 817.10 (4) | 0.2553 (5) | 184.4 (7) | 3.22 (4) | 200.1 (4) | 10.64 (7) |
| 24.2 | 815.09 (21) | 0.2554 (5) | 184.1 (7) | 3.20 (4) | 199.5 (4) | 10.55 (7) |
| 26.9 | 811.77 (30) | 0.2549 (5) | 182.6 (7) | 3.13 (4) | 199.0 (4) | 10.49 (7) |
| 30.3 | 806.36 (80) | 0.2527 (9) | 177.9 (1.3) | 2.89 (6) | 199.0 (8) | 10.50 (12) |

* For $P > 21.8$ GPa, two-phase sample.
† Fleet (1981).
‡ Calculated using the x-parameter from Fleet (1981).

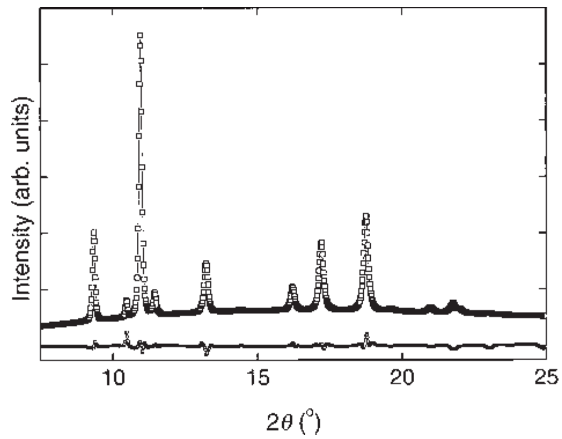


**FIGURE 3.** Observed XRD pattern of magnetite at $P$ = 12.5 GPa (top line) and the difference between observed and calculated intensities (bottom line). $\lambda$ = 47.60 pm. The small peak at around $2\theta$ = 10° belongs to $N_2$.

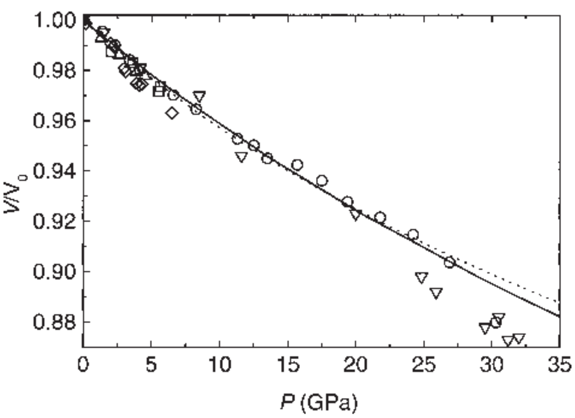


**FIGURE 4.** Variation of $V/V_0$ as a function of pressure at room temperature. Circles = present investigation; triangles = Finger et al. (1986); inverse triangles = Mao et al. (1974); squares = Staun Olsen et al. (1994); diamonds = Wilburn and Bassett (1977); solid line = the present equation of state for magnetite; dotted line = the present equation of state with $K_0$ = 198)5) and $K'_0$ = 6.7(8).

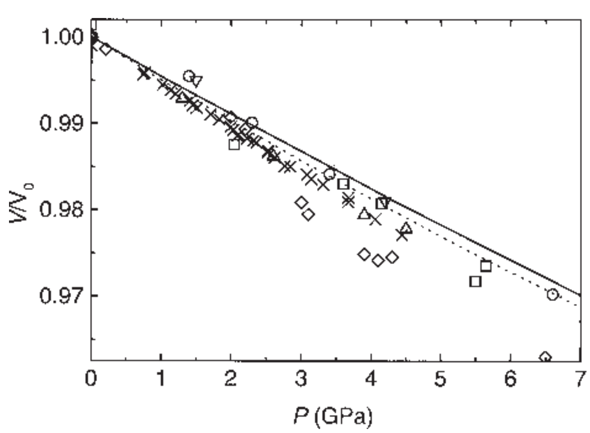


**FIGURE 5.** Variation of $V/V_0$ as a function of pressure for $P$ < 7 GPa at room temperature. See Figure 4 for symbols. In addition: × = Nakagiri et al. (1986).

squares fit of the pressure-volume data to a third order Birch-Murnaghan equation of state:

$$P = 3/2\, K_{T0}\,[(V_o/V)^{7/3} - (V_o/V)^{5/3}]\{1 - (3/4)(4 - K'_{T0})[(V_o/V)^{2/3} - 1]\} \quad (1)$$

The resulting bulk modulus and its pressure derivative are 222 (8) GPa and 4.1 (9), where the stated inaccuracy refers to the standard deviation of the fit. The bulk moduli of the cation tetrahedra and octahedra are equal to the bulk modulus characteristic of the entire crystal in agreement with the lower pressure data by Finger et al. (1986), see Figure 6. Nakagiri et al. (1986) report that tetrahedra and octahedra have different polyhedral bulk moduli values for $P$ < 4.5 GPa; 170 (10) and 200 (8) GPa, respectively.

Nine independent studies give bulk modulus values in the range from 155 to 215 GPa (Table 2). Both the pressure range covered and the pressure derivative obtained vary. The determinations by Gerward and Staun-Olsen (1995) and by Staun-Olsen et al. (1994) appear to be in agreement with the presently obtained value. A much lower value was obtained by Wilburn and Bassett (1977), whereas intermediate values are reported by Mao et al. (1974), Hazen et al. (1981), Finger et al. (1986), and Nakagiri et al. (1986).

The reason for the discrepancy between the bulk modulus presently obtained and that reported by Mao et al. (1974) is obviously related to the fact that Mao et al. (1974) included the higher-pressure determinations in their analysis. A re-evaluation based on the data by Mao et al. (1974) using data for $P$ < 20 GPa only, gives a higher bulk modulus value, $K_{T0}$ = 209 (9) GPa (for $K'_{T0}$ = 4), in good agreement with the present result. After this correction, the four studies covering $P$ > 10 GPa are in good agreement.

The bulk modulus values obtained by other techniques are in general lower than the present value. No obvious explanation is found. The pressure range of most of the earlier determinations is limited. We assume the X-ray diffraction determinations to be more reliable and the best estimate of the bulk modulus value is considered to result from an analysis taking into consideration most of the reported reduced volumes.

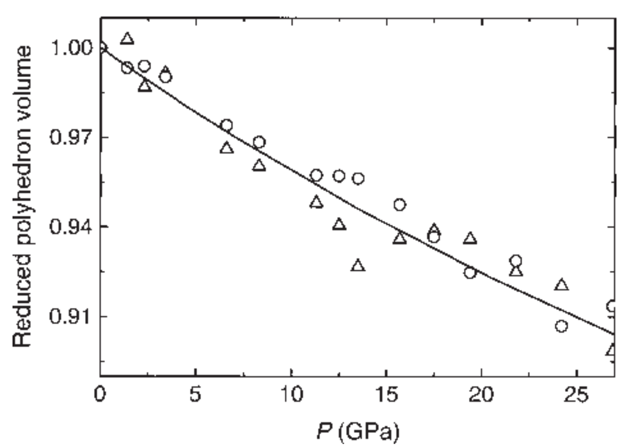


**FIGURE 6.** Variation of the reduced polyhedron volumes as a function of pressure at room temperature. Circles = octahedra; triangles = tetrahedra; solid line = the present equation of state for magnetite.

TABLE 2. Reported values of the bulk modulus of magnetite

| Reference | $K_{T0}$ GPa | $K'_{T0}$ | $P_{max}$ GPa | Sample | Method |
|---|---|---|---|---|---|
| Madelung and Fuchs (1921) | 185 (3) | – | 0.02 | bulk mineral | static compr. |
| | 175 (3) | – | 0.02 | bulk mineral | static compr. |
| Bridgman (1925) | 185 (1) | – | 1.2 | natural single cryst. | static compr. |
| Doraiswami (1947) | 162 | – | – | natural single cryst. | sonic |
| | 161 | – | – | natural single cryst. | sonic |
| Bridgman (1949) | 170 (5) | – | 2.9 | single crystal | static compr. |
| Bhagavantam (1955) | 162 | – | – | single crystal | sonic |
| Waldron (1955) | 177 | – | – | powder | IR |
| Simmons and England (1969) | 141 | – | – | – | sonic |
| | 162 | – | – | – | sonic |
| Mao et al. (1974) | 183 (10) | 4 | (0.4) | 32 | powder XRD |
| Mao et al. (1974)* | 209 (9) | 4 | 20 | powder | XRD |
| Wilburn and Bassett (1977) | 155 (12) | 4 | 6.5 | powder | XRD |
| Hazen et al. (1981) | 189 (14) | 4 | 4.5 | single cryst | XRD |
| Finger et al. (1986) | 186 (5) | 4(0.4) | 4.5 | single cryst | XRD |
| Nakagiri et al. (1986) | 181 (2) | 5.5(15) | 4.5 | single cryst | XRD |
| Staun-Olsen et al. (1994) | 200 (20) | – | 5.5 | powder | XRD |
| Gerward and Staun Olsen (1995) | 215(25) | 7.5(40) | 25 | powder | XRD |
| This work | 222(8) | 4.1(0.9) | 27 | powder | XRD |
| This work | 217(2) | 4 | 27 | selected datasets | |

*Note:* $K'_{T0}$ values of "4" are assumed.
* Subset of the dataset of Mao et al. (1974) evaluated by us.

The present data below 27 GPa is combined with those by Mao et al. (1974) below 20 GPa, and those by Nakagiri et al. (1986), by Finger et al. (1986) and by Staun-Olsen et al. (1994). Numeric data are not reported by Gerward and Staun-Olsen (1995) or by Hazen et al. (1981). The data set of Wilburn and Bassett (1977) gives an anomalous low bulk modulus value and is, hence, disregarded in the analysis. The resulting bulk modulus, given by solid lines in Figure 4 and 5, is (for $K'_{T0} = 4$) 217 (2) GPa, in agreement with the value obtained using the presently reported determinations only. An improved fit is obtained for the low-pressure region if $K'_{T0}$ is varied; giving $K'_{T0} = 6.7$ (8) and $K = 198$ (5) GPa, see dotted line in Figures 4 and 5. The solid line, representing $K'_{T0} = 4$, is considered to best describe the reduced volume against pressure curve and is used in the following discussions.

### Unit cell and equation of state of the high-pressure modification of magnetite

The observed h-$Fe_3O_4$ pattern and the available data for hematite and wüstite at around 40 GPa (Table 3; Fig. 7) suggest that the transition relates to structural rearrangements of $Fe_3O_4$ and not to decomposition of $Fe_3O_4$ to FeO + $Fe_2O_3$. Magnetite and h-$Fe_3O_4$ coexist over a large pressure range and the transition shows a considerable hysteresis. The phase transition is probably reconstructive and of first order.

A requirement for correct determination of the molar volume of the high-pressure modification is that the h-$Fe_3O_4$ reflections are properly distinguished from reflections from untransformed magnetite. Even at the highest pressures a reflection coincident with the strongest magnetite reflection at $2\theta \approx 10°$ is present (magnetite 311 line). The same reflection was observed by Fei et al. (1999), e.g., at 34 GPa and 300 K. However, their reflection disappeared on heating and it was no longer observed at 26 GPa and 723 K. This may indicate that the present sample is a two-phase mixture of magnetite and h-$Fe_3O_4$ even at the highest pressures. Still, both the increase in the FWHM and the discontinuous shift in the position for the apparent magnetite 311 above 25 GPa (Fig. 2) suggest that this reflection contains major contributions from h-$Fe_3O_4$. Furthermore, the intensity ratio between the magnetite 220 and the h-$Fe_3O_4$ reflection at $d \approx 257$ pm decreases from (1/2) to (1/90) between 30.3 and 40.0 GPa, whereas the apparent magnetite 311 reflection remains strong. In conclusion one should not neglect the possibility that there is a structural distinction between h-$Fe_3O_4$ transformed at 300 K and h-$Fe_3O_4$ subjected to subsequent annealing.

The present high-pressure diffractograms and those obtained on decompression were indexed assuming the sample to consist of two phases; $Fe_3O_4$ and $CaMn_2O_4$-type h-$Fe_3O_4$. At 24 GPa, the unit-cell dimensions for h-$Fe_3O_4$ are, $a = 278.4$ (2.4), $b = 950.6$ (5.7), and $c = 954.6$ (7.9) pm. At 23.96 GPa and 823 K, Fei et al. (1999) report the following unit-cell dimensions; $a = 279.92$ (3), $b = 940.97$ (15), and $c = 948.32$ (9) pm.

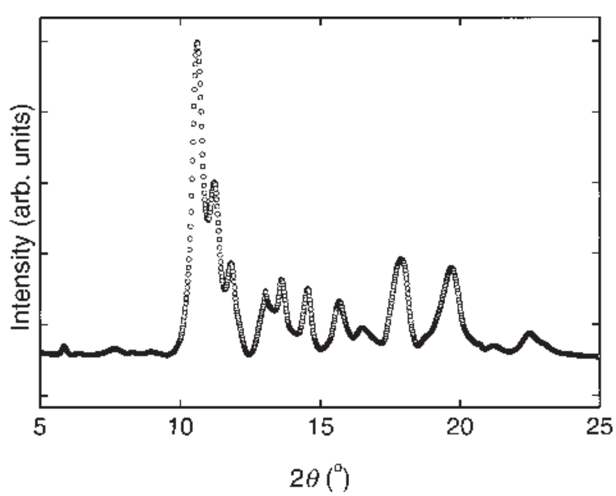


**FIGURE 7.** Observed XRD pattern of h-$Fe_3O_4$ at $P = 40$ GPa. $\lambda = 47.60$ pm.

TABLE 3. The *d*-values of the high-pressure modification of magnetite at 40.0 GPa

| This work | | | | Mao et al. (1974) | |
|---|---|---|---|---|---|
| *d*-value pm | intensity | indexing | calc. *d*-value pm | *d*-value pm | intensity |
| 466.0 | v.w. | 0 0 2/$Fe_3O_4$ | 466.6 | | |
| 354.0 | v.w. | ε - $N_2$ | | | |
| 328.0 | v.w. | 0 2 2 | 329.6 | | |
| 257.1 | st | 0 2 3* | 258.7 | 260 | 10 |
| 243.0 | m+ | $Fe_3O_4$ | | 244 | 1 |
| 230.7 | m | 1 1 2* | 230.7 | 235 | 3 |
| 226.5 | w | 0 4 1 | 226.0 | | |
| 209.4 | w+ | 0 2 4* | 208.6 | 214 | 1 |
| 200.8 | w+ | 1 3 1*/$Fe_3O_4$ | 201.8 | 203 | 4 |
| 187.9 | w+ | 1 3 2* | 189.0 | 190 | 4 |
| 174.5 | w+ | 1 1 4* | 175.2 | 179 | 2 |
| 165.8 | w– | 1 4 2 | 166.5 | | |
| 154.9 | m | 0 0 6/$Fe_3O_4$ | 155.5 | | |
| 152.9 | m | 1 5 1* | 152.5 | 155 | 4 |
| 145.8 | v.w. | 1 5 2 | 146.7 | | |
| 139.2 | m | 0 6 3* | 138.9 | 140 | 5 |
| 133.1 | v.w. | 2 2 0 | 132.7 | | |
| 129.9 | v.w. | 0 4 6 | 129.3 | | |
| 122.2 | w | 2 2 3 | 122.1 | 123 | 1 |
| 119.3 | v.w. | 1 5 5 | 119.1 | | |

*Notes:* The data taken from Mao et al. (1974) relates to $P$ = 25 GPa.
* Reflections used for calculation of unit-cell dimensions.

TABLE 4. Unit-cell parameters for h-$Fe_3O_4$

| $P$ GPa | $a$ pm | $b$ pm | $c$ pm | $V \times 10^{-6}$ pm³ |
|---|---|---|---|---|
| 40 | 275.1(1.3) | 935.0(2.8) | 932.3(3.8) | 239.8(1.6) |
| 43.5 | 274.3(1.2) | 932.3(2.8) | 928.7(3.8) | 237.5(1.6) |
| 29.5 | 276.9(2.0) | 946.9(4.7) | 947.8(6.5) | 248.5(2.8) |
| 24 | 278.4(2.4) | 950.6(5.7) | 954.6(7.9) | 252.6(3.4) |
| 18.5 | 280.4(1.8) | 954.1(4.0) | 960.1(6.5) | 256.9(2.7) |
| 12 | 282.6(2.3) | 963.4(5.4) | 967.1(7.5) | 263.3(3.3) |

The pressure-volume data are in Table 4 and in Figure 8. From these data the bulk modulus (for $K'_{T0}$ = 4) value for h-$Fe_3O_4$ was deduced, $K_{T0}$ = 202 (7) GPa. The molar volume at ambient pressure is extrapolated to 41.89 (14) cm³/mol whereas the volume decrement for the $Fe_3O_4$ to h-$Fe_3O_4$ transition at 25 GPa is 6.1%. The bulk modulus of h-$Fe_3O_4$ is slightly smaller than the one found for magnetite. In general the denser phase is expected to have a higher bulk modulus. Again the stated inaccuracy of the bulk modulus is related to the standard deviation of the fit. Considering the quality of the experimental data for h-$Fe_3O_4$ (see Table 4) and the fictive unit-cell volume at ambient conditions the true inaccuracy of the bulk modulus for h-$Fe_3O_4$ is higher.

Much higher bulk-modulus values, 340 GPa (Ahrens et al. 1969) and 450 GPa (Anderson and Kanamori 1968), have been deduced from shock-wave experiments at pressures from 65 to 130 GPa. Extrapolation to ambient pressure gave low molar volumes 38.27 cm³/mol (Ahrens et al. 1969) and 39.21 cm³/mol (Anderson and Kanamori 1968).

## Crystal structure of the high-pressure modification of magnetite

There are indications that the crystal structure of h-$Fe_3O_4$ is not a $CaMn_2O_4$-type. In $CaMn_2O_4$ the local environment around $Mn^{3+}$ is irregular due to Jahn-Teller deformation of the $MnO_6$-octahedra (Couffon et al. 1964). The high pressure form of the spinel related $Mn_3O_4$ also takes this structure type (Paris et al. 1992). In h-$Mn_3O_4$ at 39 GPa, the $Mn^{3+}$-$O^{2-}$ bond lengths for the octahedral site and the $Mn^{2+}$-$O^{2-}$ bond lengths for the eight-fold-coordinated site range from 177.2 to 223.6 pm and from 210.0 to 249.7 pm, respectively (Paris et al. 1992). In h-$Fe_3O_4$ of orthorhombic $CaMn_2O_4$-type, Fei et al. (1999) report large distortions of the cation environments. The $Fe^{3+}$-$O^{2-}$ bond lengths for the octahedral sites and the $Fe^{2+}$-$O^{2-}$ bond lengths for the eight coordinated sites at 24 GPa range from 171.5 to 258.9 pm and from 177.5 to 271.9 pm, respectively (Fei et al. 1999). Considering the $3d^n$ count for $Fe^{2+}$ and $Fe^{3+}$, no Jahn-Teller deformation is expected for Fe and the driving force for the large distortions is not easily understood. For $CaMn_2O_4$ (Couffon et al. 1964) and h-$Mn_3O_4$ (Paris et al. 1992) the variance in the Mn-O distances are modest compared with those reported for h-$Fe_3O_4$ (Fei et al. 1999). Furthermore, on the basis of bond valence considerations the crystal data for h-$Fe_3O_4$ clearly indicate charge ordering with $Fe^{2+}$ occupying a strongly deformed eight coordinated site. This appears to contradict reported $^{57}$Fe Mössbauer data (Pasternak et al. 1994).

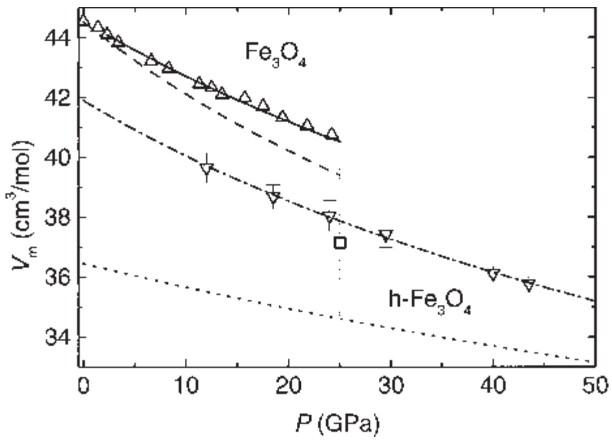


**FIGURE 8.** Molar volume of $Fe_3O_4$ as a function of pressure at ambient temperature. Triangles = present determinations for magnetite; inverse triangles = present determinations for h-$Fe_3O_4$; square = Mao et al. (1974); solid and dashed dotted lines = the presently proposed equation of state for magnetite and for h-$Fe_3O_4$; dashed line and dotted line = molar volume for magnetite and for h-$Fe_3O_4$ given by Fabrichnaya and Sundman (1997).

Despite the inferior quality of the present diffraction data, Rietveld analysis was attempted to clarify the possibility of a different structural description of h-$Fe_3O_4$. The $CaMn_2O_4$-type structure is a deformed variant of the $CaTi_2O_4$-type (Bertaut and Blum 1956) and is related to the $CaFe_2O_4$-type (Decker and Kasper 1957). These three, quite dense, structure types are compared in Figure 9. The diffraction data were clearly not consistent with the $CaFe_2O_4$-type. On turning from the deformed $CaMn_2O_4$-type to the more symmetric $CaTi_2O_4$-type, the space group symmetry is changed from *Pbcm* to *Bbmm*, however, no major changes are introduced in the unit-cell dimensions, and the volume decrement is still of the order of 6% for the magnetite to h-$Fe_3O_4$ transition. In the Rietveld refinements, the two non-equivalent iron atoms in the $CaTi_2O_4$-type description were subjected to soft distance restraints in order to secure rather

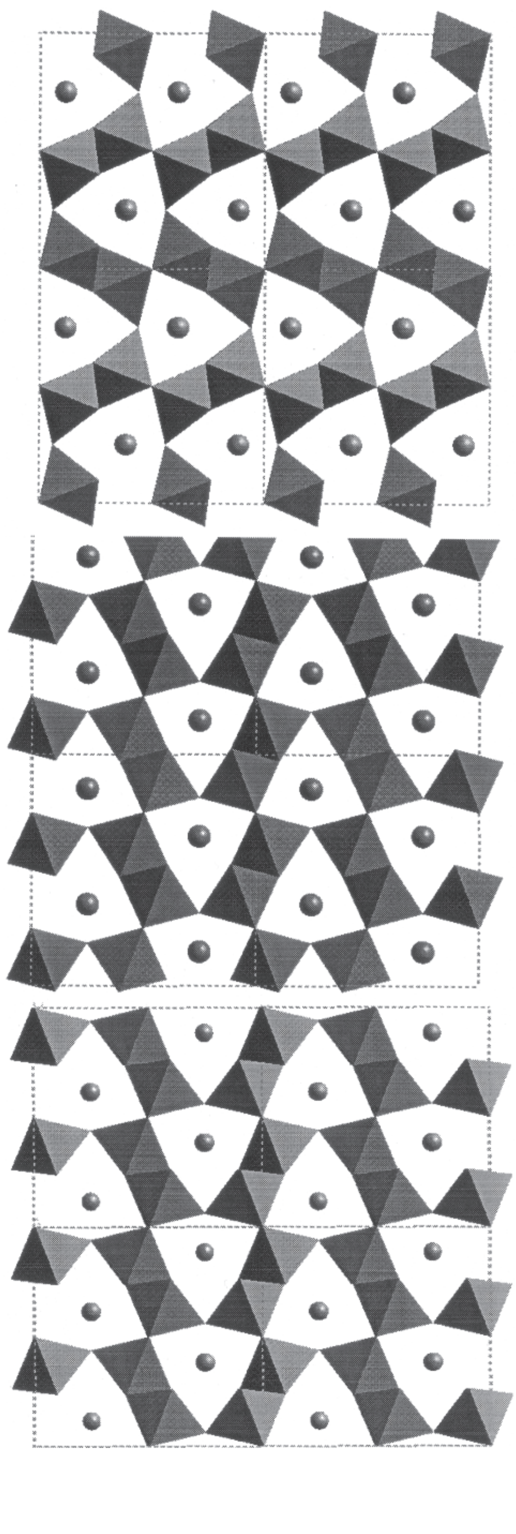

**FIGURE 9.** Comparison of the three related structure types $CaFe_2O_4$ (**upper**), $CaMn_2O_4$ (**middle**) and $CaTi_2O_4$ (**bottom**). Ca-atoms are shown as spheres, transition metal as coordination polyhedra. Projections along the short z-axis. Note that octahedra are shown for $CaMn_2O_4$ where the Jahn-Teller deformed Mn-coordination actually is 4 + 2.

symmetric Fe-O coordinations. The simulated pattern (assuming 1% strain in all directions) derived on the basis of the refined model (Fig. 10) has strong similarities with that observed by Fei et al. (1999). Proposed atomic coordinates are in Table 5. Calculated interatomic Fe-O distances are for Fe1 183 pm (×2) and 209 pm (×4), for Fe2 191 pm, 193 pm, 197 pm (×2) and 202 pm (×2). Further experiments are required in order to settle the structural ambiguity for h-$Fe_3O_4$.

## Thermodynamics of the Fe-O system at high pressure

The main motivation for the present study was the inconsistency in the thermodynamics of the Fe-O system at high pressure, which was considered to relate to the large volume decrement proposed for the magnetite to h-$Fe_3O_4$ transition (Saxena et al. 1993; Fabrichnaya and Sundman 1997). An analysis of the Fe-O system at high pressure based on the presently obtained equations of state is, hence, considered to be of interest.

The stability of $Fe_{1-y}O$, and $Fe_3O_4$ at high pressure is evaluated by assuming the phases to be stoichiometric. Inclusion of non-stoichiometry in the calculations does not affect the phase stability significantly. Our analysis is based on earlier published thermodynamic descriptions of wüstite, magnetite, and hematite at ambient pressure (Grønvold et al. 1993; Stølen et al. 1996; Stølen and Grønvold 1996). Key parameters are in Table 6. The temperature derivatives of the bulk modulus values are not known and the average value for six minerals (Anderson et al. 1991) is used. Thermodynamic descriptions of iron metal and oxygen are taken from Guillermet and Gustafson (1985)

**TABLE 5.** Atomic coordinates for the proposed crystal structure of h-$Fe_3O_4$ of $CaTi_2O_4$-type at 40 GPa

| Atom | Site | *x* | *y* | *z* |
|---|---|---|---|---|
| Fe1 | 4c | 0.375 | 0.25 | 0.00 |
| Fe2 | 8f | 0.135 | 0.087 | 0.00 |
| O1 | 4c | 0.005 | 0.25 | 0.00 |
| O2 | 8f | 0.214 | 0.605 | 0.00 |
| O3 | 4a | 0.5 | 0.00 | 0.00 |

Space group *Bbmm*, *a* = 927.3(7) pm, *b* = 923.9(4) pm, and *c* = 274.6(2) pm.

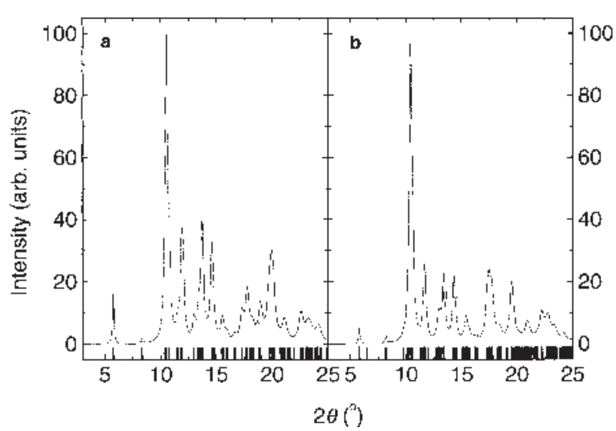


**FIGURE 10.** Simulated diffraction pattern for (**a**) h-$Fe_3O_4$ of $CaTi_2O_4$-type structure and (**b**) h-$Fe_3O_4$ of $CaMn_2O_4$-type structure according to Fei et al. (1999). λ = 47.60 pm.

TABLE 6. Thermodynamic parameters for wüstite and magnetite

| Compound | $\Delta_f H_m$(298) J/mol | $\Delta S_m$(298) J/(K·mol) | $\Delta_f G_m$(298) J/mol | $V_m$(298) cm³/mol | $K_{T_0}$ GPa |
|---|---|---|---|---|---|
| FeO | –264.06* | 60.45† | –243.52* | 12.25‡ | 150§ |
| $Fe_3O_4$ | –1115.73‖ | 146.15‖ | –1012.53‖ | 44.56 | 217 |
| h-$Fe_3O_4$ | – | – | –945.79 | 41.89 | 202 |
| $Fe_2O_3$ | –826.23* | 87.40* | –744.25* | 30.30# | 222** |

*Note:* All phases are treated as stoichiometric line compounds. $K'_{T_0}$ is assumed to equal 4.
* Stølen and Grønvold (1996).
† Stølen et al. (1996).
‡ Haas and Hemingway (1992).
§ Fei (1996).
‖ Grønvold et al. (1993).
\# Morris et al. (1981).
** Finger and Hazen (1980) and Staun-Olsen et al. (1991).

and from Belanoshko et al. (1992).

The molar volume of h-$Fe_3O_4$ is obtained from the structure proposed by Fei et al. (1999) and the presently proposed equation of state. The Gibbs energy of formation at ambient pressure but at different temperatures is obtained by shifting the Gibbs energies of formation of h-$Fe_3O_4$ reported earlier (Saxena et al. 1993) by a temperature-independent factor in order to force magnetite and h-$Fe_3O_4$ to co-exist at 25 GPa at 300 K. The resulting difference in $\Delta_f G_m$ between magnetite and h-$Fe_3O_4$ at ambient pressure at 300 K is 67 kJ/mol. Much larger $\Delta_f G_m$-differences at 300 K have been reported earlier; 161 kJ/mol (Saxena et al. 1993) and 137 kJ/mol (Fabrichnaya and Sundman 1997), see Figure 11. The equations of state proposed in the two latter studies are, hence, quite different from the present one. The molar volumes for magnetite and h-$Fe_3O_4$ are compared in Figure 8. The volume decrement of the transition at ambient pressure is presently estimated to 2.63 cm³/mol, whereas 8.08 cm³/mol results from the earlier evaluations (Saxena et al. 1993; Fabrichnaya and Sundman 1997). The present thermodynamic description gives a destabilization of h-$Fe_3O_4$ compared to earlier thermodynamic analyses, which significantly influence the calculated phase relations in the Fe-O system at high pressure.

The temperature of the eutectoid formation of wüstite from bcc-iron and magnetite decreases from 843 K at ambient pressure (Knacke 1988) to near 430 K at $P$ = 10 GPa (Fig. 12a). The temperature-pressure slope is much steeper than the one suggested by Shen et al. (1983) of –13.5 K/GPa (Fig. 12a), but it is in good agreement with the pressure variation of the transition temperature calculated from the Clausius-Clapeyron equation, $dT/dP$ = –43 K/GPa (using the molar volumes and entropies of the different phases at $T$ = 298.15 K as a first approximation). Huang and Bassett (1986) calculated the entropy of formation of wüstite from iron and magnetite at 16.5 GPa and 628 K by using the experimental $dT/dP$ and $\Delta V_m$ obtained by Shen et al. (1983). The resulting value of 44 J/(K·mol) is much larger than that obtained from experimental data at 300 K and ambient pressure, 15 J/(K·mol). An estimate of the entropy of formation of wüstite from iron and magnetite at the temperature-pressure conditions in the study by Shen et al. (1983), evaluated from the present thermodynamic description, give $\Delta_r S_m \approx$ 20 J/(K·mol). The experiments performed by Shen et al. (1983) must be considered in some detail.

According to Shen et al. (1983) wüstite forms eutectoidally from iron and magnetite when $P$ is increased to 20 GPa at 573 K.

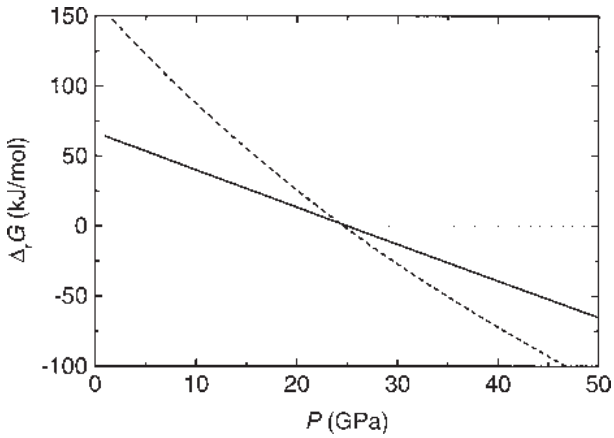


**FIGURE 11.** Gibbs energy difference between magnetite and its high-pressure modification as a function of pressure at ambient temperature. Solid line = present thermodynamic analysis; dashed line = Saxena et al. (1993).

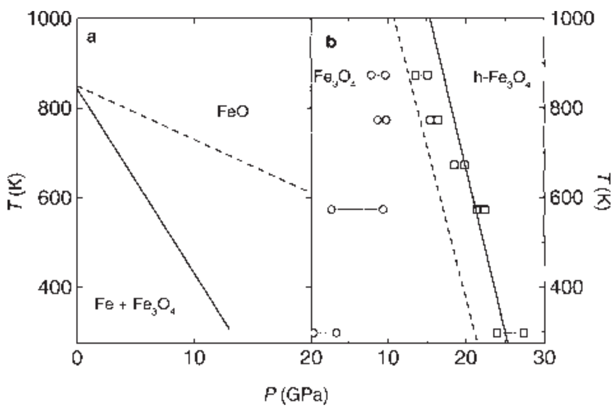


**FIGURE 12.** Phase relations in the Fe-O system. (**a**) *P-T* Phase boundary for the formation of wüstite from iron metal and magnetite. Solid line = present investigation, dashed line = Shen et al. (1983). (**b**) *P-T* Phase boundary for the formation of h-$Fe_3O_4$ from magnetite. Symbols represent experimentally determined transitional pressure intervals obtained by Huang and Bassett (1986). Squares = forward reaction, circles = reverse reaction. Solid line = present investigation; dashed line = Huang and Bassett (1986).

However, at 11, 14, and 20 GPa wüstite dominates the X-ray diffraction pattern and only small amounts of iron and magnetite are observed. On the other hand, at 6.5 GPa, iron and magnetite dominates the X-ray photographs, and only a small amount of wüstite is observed. Shen et al. (1983) suggests that the reason for the small amounts of iron and magnetite observed e.g., at 11 GPa in comparison with the much larger amounts observed at 6.5 GPa is that the difference in Gibbs energy of formation between wüstite and the stable two-phase mixture of iron and magnetite, i.e., the driving force, becomes small when the phase boundary is approached. It is tempting to suggest an alternative explanation. The presence of small amounts of iron and magnetite at 11, 14, and 20 GPa and 573 K is probably caused either by a reducing atmosphere in the diamond anvil cell or by disproportion of the high-temperature phase on cooling. We suggest that the eutectoid pressure at 573 K is in the region 6.5 to 11 GPa in good agreement with the present calculations which gives around 7 GPa.

The presently calculated *P-T* slope for the phase boundary between magnetite and its high-pressure modification (Fig. 12b), –73 K/GPa, is in reasonable agreement with experimental determination of Huang and Bassett (1986). They obtained –45 (5) K/GPa on increasing pressure and 170 (10) K/GPa on decreasing pressure and tentatively determined the equilibrium slope as –68 K/GPa when relevant kinetic effects were considered. From the volume decrement and the *P-T* slope of the magnetite to h-$Fe_3O_4$ transition, the entropy of the magnetite to h-$Fe_3O_4$ transition is calculated through the Clausius-Clapeyron equation. This large entropy of transition 34 J/(K·mol) relates to the increased coordination which lengthens and weakens the bonds in the first coordination sphere which again shifts the vibrational density of states toward lower frequencies. The earlier reported equations of state for high-magnetite based on the high bulk-modulus values deduced from shock-wave experiments and/or the structure suggested by Mao et al. (1974) give a weaker variation of the transition pressure with temperature.

The present thermodynamic description removes an earlier inconsistency in the thermodynamics of the Fe-O system at high pressure; decomposition of wüstite and the formation of (h-$Fe_3O_4$ + iron) at high pressure. Both the recently published thermodynamic descriptions by Saxena et al. (1993) and by Fabrichnaya and Sundman (1997) result in decomposition of FeO at high pressure. This is mainly due to the much higher density used for h-$Fe_3O_4$ by Saxena et al. (1993) and by Fabrichnaya and Sundman (1997).

In the preceding discussion, the relative stability of wüstite and (iron + magnetite) was considered without taking the trivalent iron oxide, hematite, into consideration. The volume decrement for the disproportion of magnetite to wüstite and hematite at ambient pressure is negative and indicates that magnetite must be expected to disproportionate on increasing the pressure. Magnetite, hence, seems to be a stable phase in the Fe-O system only for pressures below 12 GPa at ambient temperature and h-$Fe_3O_4$ appears to be metastable. High-temperature–high-pressure annealing of 15 $A^{2+}B_2^{3+}O_4$ type spinels at 12 GPa at 1273 K (Ringwood and Reid 1969) resulted in four different types of behavior. $MnAl_2O_4$, $FeAl_2O_4$, $NiAl_2O_4$, and $CoAl_2O_4$ decomposed into AO (rock salt) + $B_2O_3$ (corundum) mixtures. The driving force for the decomposition is the increased density when the spinels transform to the two-phase mixtures. $ZnAl_2O_4$, $MgAl_2O_4$, $MgCr_2O_4$, $CoGa_2O_4$, $NiGa_2O_4$, and $ZnGa_2O_4$ did not decompose at these conditions although a decomposition should be expected from the density difference between the spinels and the AO + $B_2O_3$ mixtures. The spinels are believed to be kinetically stable only and to decompose under higher pressure where the driving force for the reaction is larger (Ringwood and Reid 1969). $CdCr_2O_4$ and $CdFe_2O_4$ transforms into denser $AB_2O_4$ structures, whereas the results for $Fe_3O_4$, $ZnFe_2O_4$, $MgFe_2O_4$ were inconclusive due to partial reduction of $Fe^{3+}$ to $Fe^{2+}$ during the experiments. Further experiments are needed.

## ACKNOWLEDGMENTS

The authors gratefully acknowledges support from ESRF for travel and beam time and also financial support for CH from the Department of Chemistry, University of Oslo.

## REFERENCES CITED


Ahrens, T.J., Anderson, D.L., and Ringwood, A.E. (1969) Equations of state and crystal structures of high-pressure phases of shocked silicates and oxides. Reviews of Geophysics, 7, 667–707.

Anderson, D.L. and Kanamori, H. (1968) Shock-wave equations of state for rocks and minerals. Journal of Geophysical Research, 73, 6477–6502.

Anderson, O.L., Isaak, D.L., and Oda, H. (1991) Thermoelastic parameters for six minerals at high temperature. Journal of Geophysical Research, 96, 18037–18046.

Belonoshko, A.B., Shi, P., and Saxena, S.K. (1992) Superfluid: A FORTRAN-77 program for calculation of Gibbs free energy and volume of C-H-O-N-S-Ar mixtures. Computers and Geosciences, 18, 1267–1269.

Bertaut, E.F. and Blum, P. (1956) Détermination de la Structure de $Ti_2CaO_4$ par la Méthode Self-Consistante d'Approche Directe. Acta Crystallographica, 9, 121–126.

Bhagavantam, S. (1955) Elastic properties of single crystals and polycrystalline aggregates. Proceeding of the Indian Academy of Sciences, Section A 41, 72–90.

Bridgman, P.W. (1925) Compressiblity of fourteen natural crystals. American Journal of Science, 10, 483–498.

—— (1949) Linear compression to 30 000 kg/cm$^2$, including relatively incompressible substances. Proceedings of the American Academy of Arts and Sciences, 77, 187–234.

Couffon, M.M., Rocher, G., and Protas, M. J. (1964) Determination de la structure de la marokite. Comptes Rendus de l'Academie des Sciences, Paris, 258, 1847–1849.

Cromer, D.T., Mills, R.L., Schiferl, D., and Schwabe, L.A. (1981) The structure of $N_2$ at 49 kbar and 299 K. Acta Crystallografica, B37, 8–11.

Decker, B.F. and Kasper, J.S. (1957) The Structure of Calcium Ferrite. Acta Crystallografica, 10, 332–337.

Deslattes, R.D. and Henins, A. (1973) X-ray to visible wavelength ratios. Physical Review Letters, 31, 972–975.

Doraiswami, M.S. (1947) Elastic constants of magnetite, pyrite and chromite. Proceeding of the Indian Academy of Sciences, Section A 25, 413–416.

Fabrichnaya, O.B. and Sundman, B. (1997) The assessment of thermodynamic parameters in the Fe-O and Fe-Si-O systems. Geochimica et Cosmochimica Acta, 61, 4539–4555.

Fei, Y. (1996) Crystal chemistry of FeO at high pressure and temperature. In M.D. Dyar, C. McCammon, and M.W. Schaefer, Eds., Mineral Spectroscopy: A Tribute to Roger G. Burns, p. 243–254. The Geochemical Soceity, Special Publication No. 5.

Fei, Y. and Mao, H.K. (1994) In situ determination of the NiAs-type phase of FeO at high pressure and temperature. Science, 266, 1678–1680.

Fei, Y., Frost D.J., Mao, H.K., Prewitt, C.T., and Häusermann, D. (1999) In situ determination of the high-pressure phase of $Fe_3O_4$. American Mineralogist, 84, 203–206.

Finger, L.W. and Hazen, R.M. (1980) Crystal structure and isothermal compression of $Fe_2O_3$, $Cr_2O_3$ and $V_2O_3$ to 50 kbars. Journal of Applied Physics, 51, 5362–5367.

Finger, L.W., Hazen, R.M., and Hofmeister, A.M. (1986) High-pressure crystal chemistry of spinel ($MgAl_2O_4$) and magnetite ($Fe_3O_4$): comparisons with silicate spinels. Physics and Chemistry of Minerals, 13, 215–220.

Fleet, M.E. (1981) The structure of magnetite. Acta Crystallographica, B37, 917–920.

Gerward, L. and Staun Olsen, J. (1995) High-pressure studies of magnetite and magnesio-ferrite using synchrotron radiation. Applied Radiation Isotopes, 46, 553–554.

Grønvold, F. and Sveen, A. (1974) Heat capacity and thermodynamic properties of synthetic magnetite ($Fe_3O_4$) from 300 to 1050 K. Ferromagnetic transition and zero-point entropy. The Journal of Chemical Thermodynamics, 6, 859–872.

Grønvold, F., Stølen, S., Tolmach, P., and Westrum, E.F., Jr. (1993) Heat capacities of the wüstites $Fe_{0.9379}O$ and $Fe_{0.9254}O$ at temperatures from 5 to 350 K. Properties of $Fe_{1-y}O$ to 1000 K. Thermodynamics of formation of wüstite. The Journal of Chemical Thermodynamics, 25, 1089–1117.

Guillermet, A.F. and Gustafson, P. (1985) An assessment of the thermodynamic properties and the (P,T)-phase diagram of iron. High Temperatures-High Pressure, 16, 591–610.

Haas, J.R., Jr. and Hemingway, B.S. (1992) Recommended standard electrochemical potentials and fugacities of oxygen for the solid buffers and thermodynamic data in the systems iron-silicon-oxygen, nickel-oxygen and copper-oxygen. U.S. Geological Survey, Open file report, 92–267.

Hammersley, A.P., Svensson, S.O., Hanfland, M., Fitch, A.N., and Häusermann, D. (1996) Two-dimensional detector software: from real detector to idealized im-

age or two-theta scan. High Pressure Research, 14, 235–245.
Hazen, R.M., Finger, L.W., and Ralph, R.L. (1981) Iron oxides at high pressure: a re-evaluation of the polyhedral bulk modulus-volume relationship. EOS, 62, 416–417.
Huang, E. and Bassett, W.A. (1986) Rapid determination of $Fe_3O_4$ phase diagram by synchrotron radiation. Journal of Geophysical Research, 91, 4697–4703.
Knacke, O. (1988) The phase boundaries of wüstite. Berichte der Bunsen-Gesselschaft für Physikalische Chemie, 87, 797–800.
Larson, A.C. and von Dreele, R.B. (1986) GSAS: General structure analysis system, Los Alamos National Laboratory Report No. LAUR-86–748.
Madelung, E. and Fuchs, R. (1921) Kompressibilitätsmessungen an festen Körpern. Analen der Physik, Leipzig, Folge 4, 65, 289–309.
Mao, H.K., Takahashi, T., Bassett, W.A., Kinsland, G.L., and Merrill, L. (1974) Isothermal compression of magnetite to 320 kbar and pressure-induced phase transformation. Journal of Geophysical Research, 79, 1165–1170.
Mao, H.K., Xu, J., and Bell, P.M. (1986) Calibration of the ruby pressure gauge to 800 kbar under quasi-hydrostatic conditions. Journal of Geophysical Research, 91, 4673–4676.
Mills, R.L., Olinger, B., and Cromer, D.T. (1986) Structures and phase diagrams of $N_2$ and CO to 13 GPa by X-ray diffraction. The Journal of Chemical Physics, 84, 2837–2845.
Morris, M.C., McMurdie, H.F., Evans, E.H., Paretzkin, B., Parker, H.S., Panagiotopoulos, N.C., and Hubbard, C.R. (1981) Standard X-ray Diffraction Powder Patterns. National Bureau of Standards Monograph 25-Section, 18, p. 37.
Morris, E.R. and Williams, Q. (1997) Electrical resistivity of $Fe_3O_4$ to 48 GPa: compression-induced changes in electron hopping at mantle pressures. Journal of Geophysical Research, 102B, 18139–18148.
Nakagiri, N., Manghnani, M.H., Ming, L.C., and Kimura, S. (1986) Crystal structure of magnetite under pressure. Physics and Chemistry of Minerals, 13, 238–244.
Olijnyk, H. (1990) High pressure X-ray diffraction studies on solid $N_2$ up to 43.9 GPa. Journal of Chemical Physics, 93, 8968–8972.
Paris, E., Ross II, C.R., and Olijnyk, H. (1992) $Mn_3O_4$ at high pressure: a diamond-anvil cell study and a structural modelling. European Journal of Mineralogy, 4, 87–93.
Pasternak, M.P., Nasu, S., Wada, K., and Endo, S. (1994) High-pressure phase of magnetite. Physical Review, B50, 6446–6449.
Ramasesha, S.K., Mohan, M., Singh, A.K., Honig, J.M., and Rao, C.N.R. (1994) High-pressure study of $Fe_3O_4$ through the Verwey transition. Physical Review, 50B, 13789–13791.
Ringwood, A.E. and Reid, A.F. (1969) High pressure transformations of spinels (I). Earth and Planetary Science Letters, 5, 245–250.
Saxena, S.K., Chatterjee, N., Fei, Y., and Shen G. (1993) Thermodynamic data on oxides and silicates. Springer-Verlag, Berlin.
Shen, P., Bassett, W.A., and Liu, L. (1983) Experimental determination of the effects of pressure and temperature on the stoichiometry and phase relations of wüstite. Geochimica et Cosmochimica Acta, 47, 773–778.
Simmons, G. and England, A.W. (1969) Universal equation of state for oxides and silicates. Physics and Chemistry of Earth and Planetary Interiors, 2, 69–76.
Staun-Olsen, J., Cousins, C.S.G., Gerward, L., Jhans, H., and Sheldon, B.J. (1991) A study of the crystal structure of $Fe_2O_3$ in the pressure range up to 65 GPa using synchrotron radiation. Physica Scripta, 43, 327–330.
Staun-Olsen, J., Gerward, L., Hinze, E., and Kremmler, J. (1994) High-pressure, high-temperature study of magnetite using synchrotron radiation. Materials Science Forum, 166–169, 577–582.
Streib, W.E., Jordan, T.H., and Lipscomb, W.N. (1962) Single crystal X-ray diffraction study of β nitrogen. The Journal of Chemical Physics, 37, 2962–2965.
Stølen, S. and Grønvold, F. (1996) Calculation of the phase boundaries of wüstite at high pressure. Journal of Geophysical Research, 101B, 11531–11540.
Stølen, S., Glöckner, R., Grønvold, F. Atake, T., and Izumisawa, S. (1996) Heat capacity and thermodynamic properties of nearly stoichiometric wüstite from 13 to 450 K. American Mineralogist, 81, 973–981.
Verwey, E.J.W. (1939) Electronic conduction of magnetite ($Fe_3O_4$) and its transition point at low temperatures. Nature, 144, 327–328.
Waldron, R.D. (1955) Infrared spectra of ferrites. Physical Review, 99, 1727–1735.
Wilburn, D.R. and Bassett, W.A. (1977) Isothermal compression of magnetite ($Fe_3O_4$) up to 70 kbar under hydrostatic conditions. High Temperatures-High Pressures, 9, 35–39.
Wu, C.C. and Mason, T.O. (1981) Thermopower measurement of cation distribution in magnetite. Journal of the American Ceramic Society, 64, 520–522.

MANUSCRIPT RECEIVED MAY 5, 1999
MANUSCRIPT ACCEPTED NOVEMBER 8, 1999
PAPER HANDLED BY WILLIAM A. BASSETT